

Geophysical Research Letters[®]



RESEARCH LETTER

10.1029/2023GL104946

Tidal Modulation of Energy Dissipation Routes in the Gulf Stream

M. Contreras¹ , L. Renault¹ , and P. Marchesiello¹ 

¹LEGOS, University of Toulouse, IRD, CNRS, CNES, UPS, Toulouse, France

Key Points:

- Internal tides modulate the Gulf Stream (GS) turbulent cascade through wave-flow interaction
- External tides increase bottom drag of subtidal circulation in the deep ocean, intensifies the forward cascade
- Tide-induced increased dissipation pathways reduce GS mesoscale activity

Supporting Information:

Supporting Information may be found in the online version of this article.

Correspondence to:

M. Contreras,
marcela-paz.contreras-contreras@univ-tlse3.fr

Citation:

Contreras, M., Renault, L., & Marchesiello, P. (2023). Tidal modulation of energy dissipation routes in the Gulf Stream. *Geophysical Research Letters*, 50, e2023GL104946. <https://doi.org/10.1029/2023GL104946>

Received 19 JUN 2023

Accepted 27 SEP 2023

Author Contributions:

Conceptualization: L. Renault, P. Marchesiello

Investigation: L. Renault, P. Marchesiello
Methodology: M. Contreras, L. Renault, P. Marchesiello

Resources: L. Renault

Supervision: L. Renault, P. Marchesiello

Validation: M. Contreras

Writing – original draft: M. Contreras

Writing – review & editing: L. Renault, P. Marchesiello

© 2023. The Authors.

This is an open access article under the terms of the [Creative Commons Attribution License](https://creativecommons.org/licenses/by/4.0/), which permits use, distribution and reproduction in any medium, provided the original work is properly cited.

Abstract The Gulf Stream (GS) is a powerful ocean current that is instrumental in regulating the global climate. While a correct reproduction of GS dynamics is contingent on an appropriate representation of energy dissipation, the specific role of tides in dissipation pathways of the wind-driven circulation is not well understood. Here, we present evidence, using high-resolution ocean simulations (~2 km grid spacing), that ocean tides, by generating internal gravity waves, increase the forward cascade of energy in the GS region. This effect is greatest in summer, when the intensity of internal tides increases. However, the dissipation route associated with the forward energy cascade remains an order of magnitude weaker than frictional dissipation near the surface and bottom boundaries.

Plain Language Summary Understanding the dynamics of the Gulf Stream (GS) is essential because of its influence on global climate and ocean circulation. Previous studies have shown that a realistic representation of this region using oceanic models depends on a correct representation of the energy balance and, in particular, how the system loses energy. Energy can be dissipated at the boundaries (bottom and surface ocean) and in the interior, but how tides affect energy dissipation in the GS is unknown. In this study, we found that the interior dissipation increases when tides are included, but this route remains small compared to the energy dissipated at the boundaries.

1. Introduction

The Gulf Stream (GS) is a Western Boundary Current recognized as one of the most powerful oceanic currents. It originates in the Gulf of Mexico and the Antilles Current and transports warm water toward the pole along the U.S. East Coast from the Straits of Florida to Cape Hatteras. At Cape Hatteras, the current separates from the coast and turns northeastward. The linear Sverdrup theory predicts that the GS volume transport varies with the intensity of basin-scale wind stress curl. Numerous studies have analyzed the energy balance of this region, showing a more complex dynamic where topography and eddies exert a strong influence over a wide range of temporal and spatial scales (Chassignet & Marshall, 2008; Contreras et al., 2023b; Gula et al., 2015, 2016; Renault, Molemaker, Gula, et al., 2016; Spall, 1996; Özgökmen & Chassignet, 2002).

However, despite numerous international programs devoted to observation and modeling, our understanding of GS dynamics still has significant gaps. The GS separation from the coast has long been understood as the result of coastal curvature and the inertia required to overcome topographic steering (Debreu et al., 2022; Spall, 1996). Modeling studies of the last two decades have linked emblematic features of the GS to the resolution of mesoscale activity through eddy-mean flow interaction (McWilliams, 2008), suggesting spatial resolution of $1/10^\circ$ as a minimum for accurately representing the GS separation (Bryan et al., 2007; Chassignet & Marshall, 2008). Paradoxically, while the increase in grid resolution considerably improved the representation of the GS, the simulated eddy energy has become excessive, leading to biases in the separation of the GS as well as in its penetration of the North Atlantic basin (Chassignet & Xu, 2017; Chassignet et al., 2023; Renault, Molemaker, Gula, et al., 2016). This points to the need for a correct representation of the various energy sinks. How the energy is dissipated in the ocean has been one of the long unanswered questions. The recent literature shows that dissipation can be generated within turbulent boundary layers near the surface and bottom (Arbic et al., 2009; Ferrari & Wunsch, 2009; Renault, Molemaker, McWilliams, et al., 2016) or in the interior of the ocean (Capet et al., 2008; Contreras et al., 2023b; McWilliams, 2016; Molemaker et al., 2010).

Bottom drag represents the interaction between bottom currents and bathymetry. It is a major energy sink (Arbic et al., 2007, 2009; Nikurashin & Ferrari, 2010; Renault et al., 2023; Sen et al., 2008), controlling ocean dynamics, for example, the strength of barotropic flow and eddy-mean flow interaction (Renault et al., 2023; Trossman

et al., 2017). This is particularly true in high-energy regions like the GS (Sen et al., 2008), where bottom drag nearly balances the energy input from the wind (Weatherly, 1984). However, other dissipation processes are at work and models that fail to represent them tend to show solutions that are overly sensitive to the bottom drag parameterization (Renault et al., 2023).

Top drag is associated with frictional dissipation at the ocean surface. It actually represents the dissipation caused by the interaction between surface currents and wind stress, known as current feedback (CFB) (Renault et al., 2019; Renault, Molemaker, McWilliams, et al., 2016). CFB causes a large energy sink from (sub)mesoscale eddies to the atmosphere, damping (sub)mesoscale activity by about 30% (Renault et al., 2018; Renault, Molemaker, Gula, et al., 2016). Over the GS, the reduction of mesoscale activity weakens the eddy-flow interaction and stabilizes the mean flow, improving the representation of the GS dynamics (Renault et al., 2019).

Interior dissipation occurs with the loss of hydrostatic and geostrophic or gradient-wind momentum balances (large-scale balanced dynamics), allowing energy to be transferred to small scales (forward cascade) through to molecular dissipation (Brüggemann & Eden, 2015; Klein et al., 2008; Molemaker et al., 2010). The weakening of geostrophic balance occurs at the submesoscale, which is characterized by motions of the order of 0.1–10 km horizontally, 10–100 m vertically, and hours to days temporally (McWilliams, 2016). The associated mechanisms are: frontogenesis (Capet et al., 2008; Contreras et al., 2023b; Srinivasan et al., 2022); submesoscale quasigeostrophic instabilities at finite Rossby numbers (Capet et al., 2016); ageostrophic instabilities such as centrifugal, symmetric, gravitational, or Kelvin-Helmholtz instabilities (Contreras et al., 2019; Gula et al., 2016; Haine & Marshall, 1998; McWilliams, 2016; Thomas, 2012); and internal waves (Barkan et al., 2015; Bühler & McIntyre, 2005; Thomas, 2012). Using a 2-km resolution simulation, Contreras et al. (2023b) show that the most important energy sink for the GS is caused by top and bottom drags, and secondarily by the numerical dissipation of the model. The interior dissipation was an order of magnitude smaller than the other sinks. However, in their study, the potential effect of tides was neglected.

Internal waves can be forced by tides or winds (near-inertial waves, NIW), or generated by spontaneous emission through loss of balance, nonlinear wave-wave interactions, and lee-wave formation by geostrophic flow over sea-floor topography (Alford et al., 2016). Several studies have shown that internal waves extract energy from balanced motions, either from the mean flow or from mesoscale eddies or fronts (Barkan et al., 2015; Bühler & McIntyre, 2005; Shakespeare & Taylor, 2014; Thomas, 2012). Direct extraction is followed by wave-wave interaction, reinforcing the forward cascade (Alford et al., 2016).

Tides, more specifically, are a major source of energy for the ocean. They are caused by the gravitational forces exerted on the earth by the moon, and to a lesser extent, the sun (Stewart, 2008). The semi-diurnal M2 tide (period of 12.42 hr) is the most energetic component, accounting for around 2/3 of the energy produced by all constituents (Le Provost & Lyard, 1997; Munk & Wunsch, 1998). Tides generate strong barotropic currents, particularly in coastal waters, where around 70% of the barotropic tidal energy is dissipated by bottom drag (Egbert & Ray, 2000). The remaining 30% is transferred to internal tides in deep water over rough topography and under stratified conditions. Internal tides dissipate their energy by breaking, sometimes after traveling long distances (Garrett & Kunze, 2007). This is certainly true for semi-diurnal tides in the Atlantic, but diurnal tides are much weaker there and, because they are subinertial poleward of 30°, internal diurnal tides play only a minor role in this basin (Egbert & Ray, 2003). The transformation of internal tides during their propagation are similar to those of other internal waves: wave-wave interaction (MacKinnon & Winters, 2005); reflection, refraction and scattering by interaction with the mean flow (Duda et al., 2018; Kelly et al., 2016), or with mesoscale eddies (Rainville & Pinkel, 2006). These mechanisms suggest that internal tides can interact with the eddying wind-driven circulation and modify its energy budget, but a quantitative assessment for the entire GS system is not available. Barotropic tides, if strong enough, can also have an effect through an increase in nonlinear bottom drag, affecting both tidal and subtidal currents.

Recently, Barkan et al. (2021) has shown for a small area in the subpolar North Atlantic that internal tides tend to weaken the inverse energy cascade and strengthen the forward cascade (interior dissipation), thus reducing mesoscale kinetic energy (KE). They identify two main mechanisms: wave turbulence (the direct energy cascade of internal waves) and stimulated cascade (or imbalance), whereby internal waves trigger a transfer of energy from the mesoscale to the submesoscale. They also show that the tide-induced forward cascade is enhanced in summer, which they associate with greater M2 internal tide energy caused by increased stratification (Rocha et al., 2016). In winter, the forward cascade is stronger than in summer, but not because of internal tides, as

stratification is weakened by mixing due to winter winds and heat loss from the ocean, but because of submesoscale processes such as mixed layer instabilities that are favored by mixed layer deepening (Callies et al., 2015; Contreras et al., 2023b; Rocha et al., 2016; Schubert et al., 2020).

The main objective of this study is to analyze the effect of tides on the energy pathways of the wind-driven circulation of the GS. Firstly, we will assess the effect of tides on cross-scale KE fluxes and energy dissipation. Secondly, we will demonstrate the role of internal tides in modifying the forward cascade, but also that of surface tides in modifying bottom dissipation. A set of submesoscale-permitting simulations with tides (TD) and without tides (NTD) is analyzed for this purpose, and described in the next section.

2. Model Configuration

NTD and TD are performed with Coastal and Regional Ocean Community (CROCO; Debreu et al., 2012; Shchepetkin & McWilliams, 2005) over the period 2005–2009. The simulations are carried out in the GS region with a horizontal resolution of $1/42^\circ$ (~ 2.2 km). The NTD configuration is described in Contreras et al. (2023b). TD is similar but is additionally forced by barotropic tides (height and currents) from the global tidal model TPXOv.7 (Egbert & Erofeeva, 2002), a global tidal model that best-fits the Laplace tidal equations and altimetry data. The 8 primary harmonic components of TPXO are prescribed at the open boundaries (Marchesiello et al., 2001). In addition, the tidal potential and the self-attraction and loading—due to redistribution of water masses over the solid earth (Hendershott, 1972)—are taken from GOT99.2b, which is a global ocean tide model based on TOPEX/Poseidon altimetry (Ray, 1999), and entered as a body force throughout the CROCO domain. For top drag, both TD and NTD simulations use a stress correction approach (Renault et al., 2020). Bottom drag is quadratic and parameterized through a logarithmic law of the wall with a roughness length of $Z_{0b} = 10^{-2}$. In our analysis, 3-hr averaged output fields are used. Both NTD and TD are in good agreement with observations. This is shown for NTD in Contreras et al. (2023b) and for TD in Supporting Information S1 (SI), where we also discuss the possible effects of spatial and temporal resolution in our analysis.

3. Cross-Scale Kinetic Energy Flux

The cross-scale KE flux (Π) indicates the direction and intensity of KE transfer at a given spatial scale: positive values represent a forward cascade of energy from larger to smaller scales, while negative values represent an inverse cascade from smaller to larger scales (Aluie et al., 2018; Scott & Wang, 2005). Π is estimated here from surface currents using the coarse-graining approach (Aluie et al., 2018). Unlike the spectral analysis, the coarse-graining technique does not assume a homogeneous and isotropic field and avoids windowing procedures. In addition, this approach allows us to describe the spatial patterns of cross-scale fluxes. We follow the methodology proposed in Aluie et al. (2018) (see also Contreras et al. (2023b)) and estimate the energy flux across the spatial scales of 9, 22, and 61 km. The 9-km scale is near the effective resolution of the simulation—defined in Soufflet et al. (2016) as the dissipation wavelength below which the model KE departs from the assumed regime; 22-km marks roughly the transition between mesoscale and submesoscale in this region; and 61-km represents a peak in mesoscale activity.

Figures 1a–1c depicts the spatial average of Π in the GS region over the whole period (a), winter (b), and summer (c). The GS region is defined by the eddy kinetic energy (EKE) contour of $500 \text{ cm}^2 \text{ s}^{-2}$ estimated from AVISO dataset (Archiving, Validation and Interpretation of Oceanographic Satellite data (Ducret et al., 2000); area denoted by the black contour in Figure 2). TD, the model produces a systematic increase in the annual forward cascade at the 9- and 22-km scales compared with NTD (by 32% and 171%, respectively) and a decrease of the inverse cascade at 61 km by 42%, revealing that tides favor downscale energy transfer. Consistent with Rocha et al. (2016) and Barkan et al. (2021), the largest differences occur in summer (July–September, JAS). In summer, at 9 km, the forward cascade dominates in both simulations, but is more intense (by 148%) in TD than in NTD (Figure 1c). At the 22-km scale, the forward cascade is present only in TD, but not in NTD (where a weak inverse cascade is observed). At the 61-km scale, the inverse cascade dominates in both simulations, but is more intense in NTD than in TD (reduction of 78%). In winter (January–March, JFM), the differences are smaller but still present, reaching up to 15%, 44% and -26% at the 9, 22 and 61 km scales, respectively (Figure 1b).

In the following (and in subsequent analyses), the focus is on the summer period, that is, when the tidal influence is strongest. Similar results are obtained for the winter period or for the whole year. To better understand

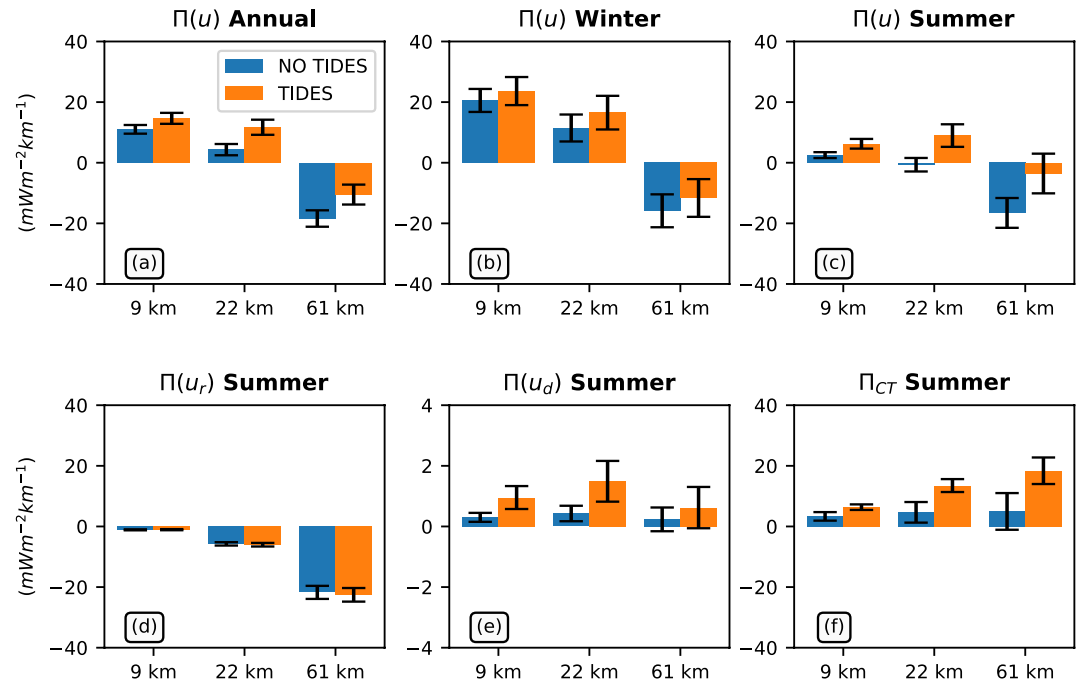


Figure 1. (a) Annual, (b) winter, and (c) summer mean cross-scale kinetic energy (KE) fluxes estimated from total surface currents in NTD and TD simulations. (d) Summer mean KE fluxes estimated from rotational currents, (e) divergent currents, and (f) the interaction of rotational and divergent currents (Π_{CT}). Note that the y-axis in (e) differs from the other graphs. In panels (a)–(f), results were spatially averaged over the Gulf Stream region defined by the black contour in Figure 2. The cross-scale fluxes are estimated at 9, 22, and 61 km. The error-bar shows the standard error estimated by the bootstrap method.

the influence of tides on the forward and inverse cascades, the surface currents are decomposed into a balanced (rotational) component \mathbf{u}_r and an unbalanced (divergent) component \mathbf{u}_d (including waves), using the Helmholtz decomposition. Contreras et al. (2023b) show that the inverse cascade is mostly explained by balanced dynamics ($\Pi(u_r)$), while the forward cascade results from unbalanced advection of balanced flow, computed as the cross-term contribution $\Pi_{CT} = \Pi - \Pi(\mathbf{u}_d) - \Pi(\mathbf{u}_r)$, where $\Pi(\mathbf{u}_d)$ is the unbalanced advection of unbalanced flow. $\Pi(\mathbf{u}_d)$ also contributes to the forward cascade, but by an order of magnitude less.

The spatial average over the GS region of the cross-scale KE flux estimated from balanced dynamics ($\Pi(\mathbf{u}_r)$) shows only a weak tidal effect on the inverse cascade at all scales analyzed (compare TD with NTD). In contrast, the two terms associated with the forward cascade, $\Pi(\mathbf{u}_d)$ and Π_{CT} , increase significantly from NTD to TD at all scales analyzed (Figures 1e and 1f). However, as with NTD, the contribution of $\Pi(\mathbf{u}_d)$ remains well below that of Π_{CT} (note that in Figure 1e, the y-axis is an order of magnitude smaller than in Figure 1f). The increase in Π_{CT} due to the tide is 91%, 189% and 270% at scales of 9, 22 and 61 km respectively. This means that the apparent reduction in the inverse cascade at 61 km and the increase in the forward cascade at 9 and 22 km are due to ageostrophic advection.

Maps of mean summer Π values in NTD and TD simulations at 9, 22, and 61 km scales are shown in Figures 2a–2c and 2d–2f, respectively. The intensification of the forward cascade in TD at all scales analyzed is produced at the GS North Wall, but mainly in the area around 40°N and 60°W, and around the Gulf of Maine (GoM). South of the GS, there is no significant change in cross-scale KE flux.

Although the GoM is not the focus here, it deserves attention because of its possible influence on the GS via tides. This region is dominated by the semi-diurnal M2 tide, greatly amplified by its unique shape, achieving one of the world's highest magnitudes. Energetic internal tides are generated by topographic interaction along the flanks of Georges Bank and propagate both onshore and offshore (Chen et al., 2011; Kelly et al., 2016). They vary with seasonal stratification changes and peak in summer, fueled by a robust pycnocline forming around 15 m deep due to solar radiation (Brown, 2011; Katavouta et al., 2016; Loder & Greenberg, 1986). The internal tides radiating

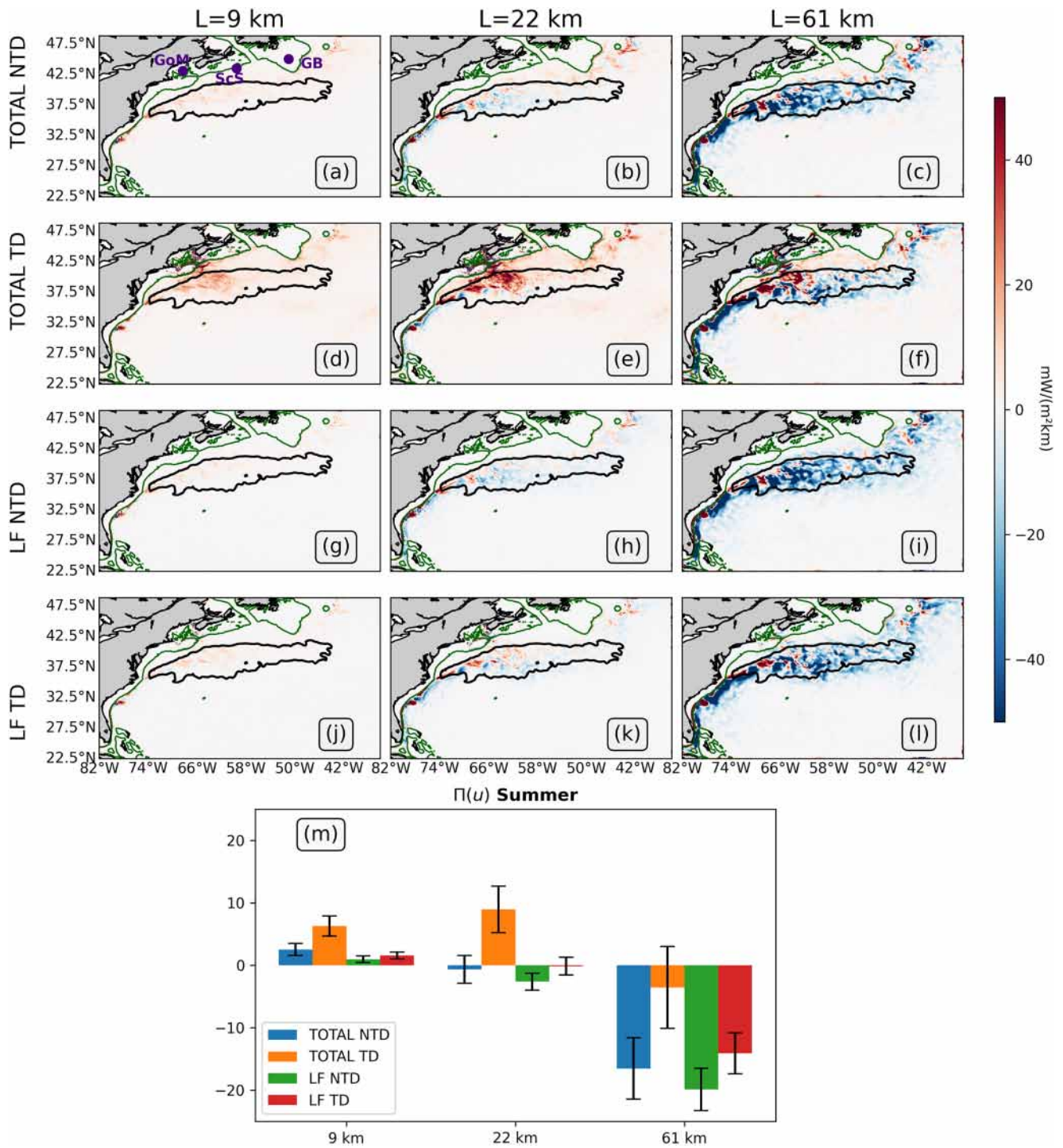


Figure 2. Maps of summer mean cross-scale kinetic energy (KE) fluxes estimated from total currents in NTD (a–c); in TD (d–f); low-frequency (>1 day) currents in NTD (LF NTD) (g–i); and in TD (LF TD) (j–l). The cross-scale fluxes are estimated at 9, 22, and 61 km. The black contour is the $500 \text{ cm}^2 \text{ s}^{-2}$ AVISO EKE contour and defines the Gulf Stream (GS) region. The green contour is the 200 m isobath. The purple dots indicate the geographic region of the Gulf of Maine, Scotian Shelf (ScS) and Grand Banks (GB). (m) Summer mean cross-scale KE fluxes estimated from TOTAL NTD (blue), TOTAL TD (orange), LF NTD (green) and LF TD (red), spatially averaged over the GS region. The error-bar in m shows the standard error estimated by the bootstrap method.

offshore can experience strong reflection and refraction by the GS (Duda et al., 2018), and tidal scattering by the mean flow that promotes energy conversion to higher modes (Dunphy & Lamb, 2014; Kelly et al., 2016). Noteworthy, the region where the forward cascade is greatest in TD (around 40°N and 60°W), coincides with the location of GS-altered non-coherent internal tides reported by Kelly et al. (2016) (see their Figure 12).

4. Role of Internal Tides

The increase of the forward KE cascade from NTD to TD simulations could be explained by the generation of internal tides. To verify this hypothesis, we decomposed the TD surface currents into their high-frequency and low-frequency components, assuming that high-frequency currents are associated with internal tides (off the shelf). To obtain the low-frequency component ($\hat{\mathbf{u}}$), we apply a temporal Butterworth low-pass filter with a cutoff period of 1-day. The high-frequency component is defined as $\mathbf{u}'' = \mathbf{u} - \hat{\mathbf{u}}$. Comparison of the spectra indicates that the filter effectively eliminates the tidal signal (not shown). However, one of the main caveats of this methodology is that it also suppresses waves generated by other mechanisms and probably some high-frequency submesoscale currents.

As in the previous section, our analysis focuses on summer. Using $\hat{\mathbf{u}}$ from TD, we estimated the associated KE flux ($\Pi(\hat{\mathbf{u}})$). $\Pi(\hat{\mathbf{u}})$ shows a weaker forward cascade than the total flux Π (Figures 2d–2f), especially over the GoM and around 40°N and 60°W. Interestingly, the magnitude of $\Pi(\hat{\mathbf{u}})$ in TD is comparable to Π in NTD at all scales (Figures 2a–2c). This confirms that the internal tides are responsible for the intensification of the forward cascade.

Comparison of filtered and unfiltered KE fluxes in TD shows that $\Pi(\hat{\mathbf{u}})$ (Figure 2j) is reduced by 75% compared to Π (Figure 2d) at the 9 km scale. At the 22-km scale, the reduction is 101% (Figures 2e and 2k). At this scale, Π shows an intense forward cascade, which is higher than that at the 9 km scale, in stark contrast to $\Pi(\hat{\mathbf{u}})$ which shows a weak inverse cascade.

Although the filtered KE flux in TD is similar to the total flux in NTD, as mentioned above, $\Pi(\hat{\mathbf{u}})$ in TD (Figure 2j) is, however, 38% lower than Π in NTD at the 9 km scale (Figure 2a). At the 22 and 61 km scales, $\Pi(\hat{\mathbf{u}})$ in TD also shows a reduction in the inverse cascade of 74% and 14% compared to NTD, respectively. This difference is explained by the removal of internal waves generated by non-tidal mechanisms, which are present in both TD and NTD. The contribution of non-tidal mechanisms can be revealed by calculating $\Pi(\hat{\mathbf{u}})$ in NTD with the same filters. In summer, in the GS region, the forward cascade at 9-km scale given by $\Pi(\hat{\mathbf{u}})$ in NTD is reduced by 62% compared to Π . At 22 and 61-km scales, the inverse cascade given by $\Pi(\hat{\mathbf{u}})$ in NTD is increased by 299% and 20%, respectively. These results suggest that non-tidal waves contribute significantly to the forward cascade. However, note that some of the filtered high-frequency currents belong to submesoscale eddies rather than transient features such as wind-generated NIWs.

In summary, high-frequency currents are relevant to explain the forward cascade induced by tides. It seems that the intensification of the forward cascade around 40°N and 60°W results from the interaction between the internal tides generated in the GoM and the mean GS flow (see previous section). It should be noted that the forward cascade is also intensified by high-frequency currents in areas close to the Scotian Shelf and Grand Banks (indicated in Figures 2a–2f). However, this enhancement is less significant than that observed around 40°N and 60°W, possibly due to weaker tides and currents.

5. Energy Sink

Here, we evaluate the overall impact of tides on the energy sinks following the methodology proposed in Contreras et al. (2023b):

- Dissipation of mesoscale currents by top drag can be estimated using the eddy geostrophic wind work $F_e K_e = \langle \mathbf{u}'_g \tau' \rangle - \Pi_{\tau_{22km}}$ where $\langle \rangle$ and \prime operators indicate the average over 3-month and its fluctuation, respectively, and $\Pi_{\tau_{22km}} = \overline{\tau \cdot \mathbf{u}_g} - \overline{\tau} \cdot \overline{\mathbf{u}_g}$ is the coarse-grained wind work at 22-km.
- Dissipation by bottom drag is computed from the covariance of the bottom currents and bottom stress anomalies $F_b K_b = \langle \mathbf{u}'_b \tau'_b \rangle$.
- Interior dissipation is defined as $I_{Diss} = - \int_{-100m}^{surface} \Pi_{9km} dz$.

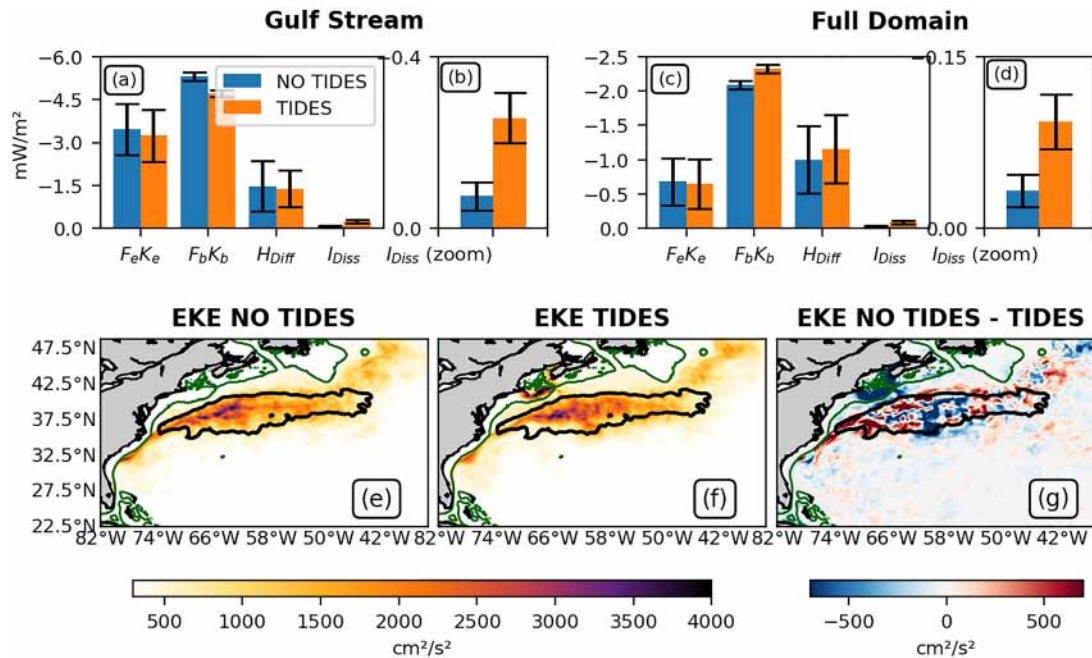


Figure 3. Summer mean kinetic energy dissipation computed from NTD (blue bar) and TD (orange bar) and spatially averaged over panels (a)–(b) the Gulf Stream region defined by the black outline in (e)–(g) and (c)–(d) the entire domain. Panels (b), (d) are zoom panels of panels (a) and (b) for I_{Diss} . In each panel, the error-bar shows the standard error estimated by the bootstrap method. Panels (e)–(g) Summer mean EKE estimated from NTD, TD, and their difference. The green contour is the 200 m isobath.

- We estimate numerical dissipation (from the fifth-order upstream scheme, UP5, used in the simulations) $H_{Diff} = \int_{bottom}^{surface} \mathbf{u} \cdot D dz$, where D is the horizontal momentum diffusion diagnosed from the difference between UP5 and a non-dissipative sixth-order centered scheme (Contreras et al., 2023b).

Negative values of these diagnostics indicate a dissipation of energy. Again, the energy sink terms are estimated for summer (similar results are found for the other seasons or the whole year).

The average over the GS region (and over the whole domain) reveals that the major contribution to energy dissipation in TD and NTD is produced by top and bottom drag, followed by numerical dissipation (Figures 3a–3d). Consistent with Contreras et al. (2023b), the contribution of the interior dissipation is an order of magnitude smaller than the other energy sinks. Over the GS region, $F_b K_b$ is reduced by 11% between NTD and TD (Figure 3a). A slight decrease of 6% in TD is also shown in both $F_e K_e$ and H_{Diff} . As expected from our previous results, including the tides leads to an increase of I_{Diss} by 240% (stronger forward cascade; Figures 3a and 3b). However, I_{Diss} remains an order of magnitude smaller than the other sinks.

One possible reason for the decrease in energy dissipation over the GS region in TD is the decrease in eddy KE (EKE; where perturbations are measured as deviations from the 3-month mean), in particular from Cape Hatteras to 60°W (Figure 3g). Paradoxically, the reduction of EKE is caused by increased dissipation by barotropic tides over the entire domain, which stabilizes the GS and thus reduces energy conversion to mesoscale eddies. We noted a 2.35% reduction in EKE over the entire domain (and a 0.23% reduction over the GS). Although these percentages seem small, a strong correspondence is found between the NTD-TD EKE difference (Figure 1g) and the NTD-TD $F_b K_b$ difference (not shown). A positive difference in EKE translates into a negative difference in $F_b K_b$, with an estimated correlation coefficient of -0.6 . Over the entire deep ocean domain (i.e., the area deeper than 200 m, corresponding to the thick dark green line in Figure 2), $F_b K_b$, H_{Diff} and I_{Diss} increase by 11%, 15%, and 182%, respectively, when tides are present (TD).

6. Discussion and Conclusion

In this study, we described the effects of tides on the KE pathway of the GS using two submesoscale permitting (2 km) ocean models, TD and NTD. We analyzed the cross-scale KE flux using a coarse-graining approach.

Although significant throughout the year, the impact of tides on energy transfer seems to be greatest in summer, which is in line with Rocha et al. (2016), Barkan et al. (2021). In summer, over the GS region, the cross-scale KE flux from the tidal simulation shows a decrease in the inverse cascade and an increase in the forward cascade, which is explained by an increase in unbalanced (ageostrophic) advection.

A decomposition between high-frequency and low-frequency currents (≥ 1 day) shows that the intensification of the forward cascade in TD is mainly driven by internal tides. When the high-frequency currents are filtered out, the cross-scale KE flux in TD is much closer to that estimated in NTD. The remaining difference can be attributed to non-tidal features (NIW and high-frequency range of submesoscale eddies) and possibly, to a lesser extent, to the residual tidal signals, imperfectly eliminated by the temporal filter.

Previous studies have suggested that wave-wave and wave-flow interactions can both produce a forward cascade (Alford et al., 2016). If we associate Π_{CT} (unbalanced advection of balanced flow) with wave-flow interaction and $\Pi(\mathbf{u}_d)$ (unbalanced advection of unbalanced flow) with wave-wave interaction, and since $\Pi_{CT} \gg \Pi(\mathbf{u}_d)$, we confirm here that wave-flow interaction has the greatest contribution to the forward cascade. This is also supported by the forward cascade intensification around 40°N and 60°W (Figure 2) where significant interaction between internal tides and the GS has been suggested by Kelly et al. (2016). The specific mechanisms involved in the wave-flow interaction are unclear, but Π_{CT} is consistent with the stimulated imbalance process proposed by Barkan et al. (2017), where externally forced internal waves stimulates a transfer of energy from mesoscale to submesoscale eddies. Future work should attempt to clarify this point.

In winter, the impact of the tides is the same as in summer, but less intense, that is, the intensification (weakening) of the forward (inverse) cascade is lower. The forward cascade without the contribution of internal waves (generated by both tides and winds) decreases by 47% and 26% at 9 and 22 km scales (where the forward cascade dominates). These numbers are lower than in summer, but are significant.

Early tidal models were decoupled to the wind-driven ocean general circulation (Hendershott, 1972; Hibiya et al., 2006; Simmons, 2008). It is now more common to use models that combine the two dynamics, such as CROCO (Barkan et al., 2021; Delpech et al., 2023; Renault & Marchesiello, 2022), Massachusetts Institute of Technology general circulation model (MITgcm; Rocha et al., 2016), and Hybrid Coordinate Ocean Model (HYCOM; Arbic et al., 2010). The inclusion of tides improves the representation of low-frequency ocean dynamics (Arbic et al., 2012; Chavanne et al., 2010; Padman et al., 2006; Park & Watts, 2006), but regional ocean models often fail to accurately reproduce high-frequency observations (Kumar et al., 2019; Mazloff et al., 2020; Nelson et al., 2020; Siyanbola et al., 2023). Here too, internal tides and their effects may be under-represented. One possible improvement is to include the forcing of remotely generated internal tides in the open boundary conditions (Nelson et al., 2020; Siyanbola et al., 2023). However, care must be taken when implementing the boundary conditions to avoid excessive reflection of internal waves from the interior, which would falsely increase the internal wave energy (Siyanbola et al., 2023).

Despite possible caveats in the methodology, the present results convincingly assess the role that tides would play in the energy balance of the GS circulation. They demonstrate a large change in the turbulent cascade, although the forward cascade as a dissipation pathway remains weaker than frictional dissipation near surface and bottom boundaries. Besides, bottom dissipation of the subtidal circulation is also increased by barotropic tides in the deep ocean, which may seem contradictory to the assumption that barotropic tides in the deep ocean decay mainly by conversion to baroclinic tides (Egbert & Ray, 2003). Overall, our results seem to confirm that the ocean's KE tends to dissipate mainly near its boundaries, and that ocean models should probably pay more attention to the treatment of bottom topography and friction, air-sea coupling processes and numerical dissipation.

Data Availability Statement

CROCO model is available at Auclair et al. (2022). The data to reproduce the figures are available at Contreras et al. (2023a).

Acknowledgments

M. Contreras was supported by Becas Chile from ANID (Agencia Nacional de Investigación y Desarrollo); CONICYT-PFCHA/Doctorado Becas Chile/2020-72210196). We appreciate support from the Centre National d'Étude Spatial through the TOSCA projects I-CASCADE and M-ODYSEA, and from LEFE VENUS and the GdR CROCO and GdRI CROCO. The model and calculations were executed at GENCI (project 13051). We appreciate the suggestions of the two anonymous reviewers, which improved the quality of our manuscript.

References

Alford, M. H., MacKinnon, J. A., Simmons, H. L., & Nash, J. D. (2016). Near-inertial internal gravity waves in the ocean. *Annual Review of Marine Science*, 8(1), 95–123. <https://doi.org/10.1146/annurev-marine-010814-015746>

Aluie, H., Hecht, M., & Vallis, G. K. (2018). Mapping the energy cascade in the North Atlantic Ocean: The coarse-graining approach. *Journal of Physical Oceanography*, 48(2), 225–244. <https://doi.org/10.1175/jpo-d-17-0100.1>

Arbic, B. K., Flierl, G. R., & Scott, R. B. (2007). Cascade inequalities for forced–dissipated geostrophic turbulence. *Journal of Physical Oceanography*, 37(6), 1470–1487. <https://doi.org/10.1175/jpo3067.1>

Arbic, B. K., Richman, J. G., Shriver, J. F., Timko, P. G., Metzger, E. J., & Wallcraft, A. J. (2012). Global modeling of internal tides: Within an eddy ocean general circulation model. *Oceanography*, 25(2), 20–29. <https://doi.org/10.5670/oceanog.2012.38>

Arbic, B. K., Shriver, J. F., Hogan, P. J., Hurlburt, H. E., McClean, J. L., Metzger, E. J., et al. (2009). Estimates of bottom flows and bottom boundary layer dissipation of the oceanic general circulation from global high-resolution models. *Journal of Geophysical Research*, 114(C2), C02024. <https://doi.org/10.1029/2008jc005072>

Arbic, B. K., Wallcraft, A. J., & Metzger, E. J. (2010). Concurrent simulation of the eddy ocean general circulation and tides in a global ocean model. *Ocean Modelling*, 32(3–4), 175–187. <https://doi.org/10.1016/j.ocemod.2010.01.007>

Auclair, F., Benschila, R., Bordoio, L., Boutet, M., Brémond, M., Caillaud, M., et al. (2022). Coastal and regional ocean community model [Software]. Zenodo. <https://doi.org/10.5281/zenodo.7415343>

Barkan, R., Srinivasan, K., Yang, L., McWilliams, J. C., Gula, J., & Vic, C. (2021). Oceanic mesoscale eddy depletion catalyzed by internal waves. *Geophysical Research Letters*, 48(18), e2021GL094376. <https://doi.org/10.1029/2021gl094376>

Barkan, R., Winters, K. B., & McWilliams, J. C. (2017). Stimulated imbalance and the enhancement of eddy kinetic energy dissipation by internal waves. *Journal of Physical Oceanography*, 47(1), 181–198. <https://doi.org/10.1175/jpo-d-16-0117.1>

Barkan, R., Winters, K. B., & Smith, S. G. L. (2015). Energy cascades and loss of balance in a reentrant channel forced by wind stress and buoyancy fluxes. *Journal of Physical Oceanography*, 45(1), 272–293. <https://doi.org/10.1175/jpo-d-14-0068.1>

Brown, W. (2011). Winter variability in the western gulf of Maine: Part I: Internal tides. *Dynamics of Atmospheres and Oceans*, 52(1–2), 224–249. <https://doi.org/10.1016/j.dynatmoce.2011.03.004>

Brüggemann, N., & Eden, C. (2015). Routes to dissipation under different dynamical conditions. *Journal of Physical Oceanography*, 45(8), 2149–2168. <https://doi.org/10.1175/jpo-d-14-0205.1>

Bryan, F. O., Hecht, M. W., & Smith, R. D. (2007). Resolution convergence and sensitivity studies with North Atlantic circulation models. Part I: The western boundary current system. *Ocean Modelling*, 16(3–4), 141–159. <https://doi.org/10.1016/j.ocemod.2006.08.005>

Bühler, O., & McIntyre, M. E. (2005). Wave capture and wave–vortex duality. *Journal of Fluid Mechanics*, 534, 67–95. <https://doi.org/10.1017/s0022112005004374>

Callies, J., Ferrari, R., Klymak, J. M., & Gula, J. (2015). Seasonality in submesoscale turbulence. *Nature Communications*, 6(1), 6862. <https://doi.org/10.1038/ncomms7862>

Capet, X., McWilliams, J. C., Molemaker, M. J., & Shchepetkin, A. F. (2008). Mesoscale to submesoscale transition in the California current system. Part III: Energy balance and flux. *Journal of Physical Oceanography*, 38(10), 2256–2269. <https://doi.org/10.1175/2008jpo3810.1>

Capet, X., Rouillet, G., Klein, P., & Maze, G. (2016). Intensification of upper-ocean submesoscale turbulence through charney baroclinic instability. *Journal of Physical Oceanography*, 46(11), 3365–3384. <https://doi.org/10.1175/jpo-d-16-0050.1>

Chassignet, E. P., & Marshall, D. P. (2008). Gulf stream separation in numerical ocean models. In *Geophysical Monograph Series* (Vol. 177).

Chassignet, E. P., & Xu, X. (2017). Impact of horizontal resolution (1/12 to 1/50) on gulf stream separation, penetration, and variability. *Journal of Physical Oceanography*, 47(8), 1999–2021. <https://doi.org/10.1175/jpo-d-17-0031.1>

Chassignet, E. P., Xu, X., Bozec, A., & Uchida, T. (2023). Impact of the New England seamount chain on gulf stream pathway and variability. *Journal of Physical Oceanography*, 53(8), 1871–1886. <https://doi.org/10.1175/jpo-d-23-0008.1>

Chavanne, C., Flament, P., Luther, D., & Gurgel, K. (2010). The surface expression of semidiurnal internal tides near a strong source at Hawaii. Part II: Interactions with mesoscale currents. *Journal of Physical Oceanography*, 40(6), 1180–1200. <https://doi.org/10.1175/2010jpo4223.1>

Chen, C., Huang, H., Beardsley, R. C., Xu, Q., Limeburner, R., Cowles, G. W., et al. (2011). Tidal dynamics in the gulf of Maine and New England shelf: An application of FVCOM. *Journal of Geophysical Research*, 116(C12), C12010. <https://doi.org/10.1029/2011jgc007054>

Contreras, M., Pizarro, O., Dewitte, B., Sepulveda, H. H., & Renault, L. (2019). Subsurface mesoscale eddy generation in the ocean off Central Chile. *Journal of Geophysical Research: Oceans*, 124(8), 5700–5722. <https://doi.org/10.1029/2018jc014723>

Contreras, M., Renault, L., & Marchesiello, P. (2023a). Tidal modulation of cross-scale kinetic energy fluxes in the gulf stream [Dataset]. Figshare. <https://doi.org/10.6084/m9.figshare.23393267>

Contreras, M., Renault, L., & Marchesiello, P. (2023b). Understanding energy pathways in the gulf stream. *Journal of Physical Oceanography*, 53(3), 719–736. <https://doi.org/10.1175/jpo-d-22-0146.1>

Debreu, L., Kevlahan, N.-R., & Marchesiello, P. (2022). Improved gulf stream separation through brinkman penalization. *Ocean Modelling*, 179, 102121. <https://doi.org/10.1016/j.ocemod.2022.102121>

Debreu, L., Marchesiello, P., Penven, P., & Cambon, G. (2012). Two-way nesting in split-explicit ocean models: Algorithms, implementation and validation. *Ocean Modelling*, 49, 1–21. <https://doi.org/10.1016/j.ocemod.2012.03.003>

Delpech, A., Barkan, R., Renault, L., McWilliams, J., Siyanbola, O. Q., Buijsman, M. C., & Arbic, B. K. (2023). Wind-current feedback is an energy sink for oceanic internal waves. *Scientific Reports*, 13(1), 5915. <https://doi.org/10.1038/s41598-023-32909-6>

Ducet, N., Le Traon, P. Y., & Reverdin, G. (2000). Global high-resolution mapping of ocean circulation from TOPEX/Poseidon and ERS-1 and -2. *Journal of Geophysical Research*, 105(C8), 19477–19498. <https://doi.org/10.1029/2000jc900063>

Duda, T. F., Lin, Y.-T., Buijsman, M., & Newhall, A. E. (2018). Internal tidal modal ray refraction and energy ducting in baroclinic gulf stream currents. *Journal of Physical Oceanography*, 48(9), 1969–1993. <https://doi.org/10.1175/jpo-d-18-0031.1>

Dunphy, M., & Lamb, K. G. (2014). Focusing and vertical mode scattering of the first mode internal tide by mesoscale eddy interaction. *Journal of Geophysical Research: Oceans*, 119(1), 523–536. <https://doi.org/10.1002/2013jc009293>

Egbert, G. D., & Erofeeva, S. Y. (2002). Efficient inverse modeling of Barotropic Ocean tides. *Journal of Atmospheric and Oceanic Technology*, 19(2), 183–204. [https://doi.org/10.1175/1520-0426\(2002\)019<0183:eimoboz>2.0.co;2](https://doi.org/10.1175/1520-0426(2002)019<0183:eimoboz>2.0.co;2)

Egbert, G. D., & Ray, R. D. (2000). Significant dissipation of tidal energy in the deep ocean inferred from satellite altimeter data. *Nature*, 405(6788), 775–778. <https://doi.org/10.1038/35015531>

Egbert, G. D., & Ray, R. D. (2003). Semi-diurnal and diurnal tidal dissipation from topex/poseidon altimetry. *Geophysical Research Letters*, 30(17), 1907. <https://doi.org/10.1029/2003gl017676>

Ferrari, R., & Wunsch, C. (2009). Ocean circulation kinetic energy: Reservoirs, sources, and sinks. *Annual Review of Fluid Mechanics*, 41(1), 253–282. <https://doi.org/10.1146/annurev.fluid.40.1.11406.102139>

- Garrett, C., & Kunze, E. (2007). Internal tide generation in the deep ocean. *Annual Review of Fluid Mechanics*, 39(1), 57–87. <https://doi.org/10.1146/annurev.fluid.39.050905.110227>
- Gula, J., Molemaker, M. J., & McWilliams, J. C. (2015). Gulf stream dynamics along the southeastern us seaboard. *Journal of Physical Oceanography*, 45(3), 690–715. <https://doi.org/10.1175/jpo-d-14-0154.1>
- Gula, J., Molemaker, M. J., & McWilliams, J. C. (2016). Submesoscale dynamics of a gulf stream frontal eddy in the South Atlantic bight. *Journal of Physical Oceanography*, 46(1), 305–325. <https://doi.org/10.1175/jpo-d-14-0258.1>
- Haine, T. W. N., & Marshall, J. (1998). Gravitational, symmetric, and baroclinic instability of the ocean mixed layer. *Journal of Physical Oceanography*, 28(4), 634–658. [https://doi.org/10.1175/1520-0485\(1998\)028<0634:gsabio>2.0.co;2](https://doi.org/10.1175/1520-0485(1998)028<0634:gsabio>2.0.co;2)
- Hendershott, M. (1972). The effects of solid Earth deformation on global ocean tides. *Geophysical Journal International*, 29(4), 389–402. <https://doi.org/10.1111/j.1365-246x.1972.tb06167.x>
- Hibiya, T., Nagasawa, M., & Niwa, Y. (2006). Global mapping of diapycnal diffusivity in the deep ocean based on the results of expendable current profiler (XCP) surveys. *Geophysical Research Letters*, 33(3), L03611. <https://doi.org/10.1029/2005gl025218>
- Katavouta, A., Thompson, K. R., Lu, Y., & Loder, J. W. (2016). Interaction between the tidal and seasonal variability of the gulf of Maine and Scotian shelf region. *Journal of Physical Oceanography*, 46(11), 3279–3298. <https://doi.org/10.1175/jpo-d-15-0091.1>
- Kelly, S. M., Lermusiaux, P. F., Duda, T. F., & Haley, P. J., Jr. (2016). A coupled-mode shallow-water model for tidal analysis: Internal tide reflection and refraction by the gulf stream. *Journal of Physical Oceanography*, 46(12), 3661–3679. <https://doi.org/10.1175/jpo-d-16-0018.1>
- Klein, P., Hua, B. L., Lapeyre, G., Capet, X., Le Gentil, S., & Sasaki, H. (2008). Upper ocean turbulence from high-resolution 3d simulations. *Journal of Physical Oceanography*, 38(8), 1748–1763. <https://doi.org/10.1175/2007jpo3773.1>
- Kumar, N., Suanda, S. H., Colosi, J. A., Haas, K., Di Lorenzo, E., Miller, A. J., & Edwards, C. A. (2019). Coastal semidiurnal internal tidal incoherence in the Santa Maria basin, California: Observations and model simulations. *Journal of Geophysical Research: Oceans*, 124(7), 5158–5179. <https://doi.org/10.1029/2018jc014891>
- Le Provost, C., & Lyard, F. (1997). Energetics of the M_2 Barotropic Ocean tides: An estimate of bottom friction dissipation from a hydrodynamic model. *Progress in Oceanography*, 40(1–4), 37–52. [https://doi.org/10.1016/s0079-6611\(97\)00022-0](https://doi.org/10.1016/s0079-6611(97)00022-0)
- Loder, J. W., & Greenberg, D. A. (1986). Predicted positions of tidal fronts in the gulf of Maine region. *Continental Shelf Research*, 6(3), 397–414. [https://doi.org/10.1016/0278-4343\(86\)90080-4](https://doi.org/10.1016/0278-4343(86)90080-4)
- MacKinnon, J. A., & Winters, K. (2005). Subtropical catastrophe: Significant loss of low-mode tidal energy at 28.9°. *Geophysical Research Letters*, 32(15), L15605. <https://doi.org/10.1029/2005gl023376>
- Marchesiello, P., McWilliams, J. C., & Shchepetkin, A. (2001). Open boundary conditions for long-term integration of regional oceanic models. *Ocean Modelling*, 3(1–2), 1–20. [https://doi.org/10.1016/s1463-5003\(00\)00013-5](https://doi.org/10.1016/s1463-5003(00)00013-5)
- Mazloff, M. R., Cornuelle, B., Gille, S. T., & Wang, J. (2020). The importance of remote forcing for regional modeling of internal waves. *Journal of Geophysical Research: Oceans*, 125(2), e2019JC015623. <https://doi.org/10.1029/2019jc015623>
- McWilliams, J. C. (2008). The nature and consequences of oceanic eddies. *Ocean Modeling in an Eddy Regime*, 177, 5–15.
- McWilliams, J. C. (2016). Submesoscale currents in the ocean. *Proceedings of the Royal Society A: Mathematical, Physical and Engineering Sciences*, 472(2189), 20160117. <https://doi.org/10.1098/rspa.2016.0117>
- Molemaker, M. J., McWilliams, J. C., & Capet, X. (2010). Balanced and unbalanced routes to dissipation in an equilibrated eddy flow. *Journal of Fluid Mechanics*, 654, 35–63. <https://doi.org/10.1017/s002212009993272>
- Munk, W., & Wunsch, C. (1998). Abyssal recipes II: Energetics of tidal and wind mixing. *Deep Sea Research Part I: Oceanographic Research Papers*, 45(12), 1977–2010. [https://doi.org/10.1016/s0967-0637\(98\)00070-3](https://doi.org/10.1016/s0967-0637(98)00070-3)
- Nelson, A., Arbic, B., Menemenlis, D., Peltier, W., Alford, M., Grisouard, N., & Klymak, J. (2020). Improved internal wave spectral continuum in a regional ocean model. *Journal of Geophysical Research: Oceans*, 125(5), e2019JC015974. <https://doi.org/10.1029/2019jc015974>
- Nikurashin, M., & Ferrari, R. (2010). Radiation and dissipation of internal waves generated by geostrophic motions impinging on small-scale topography: Application to the southern ocean. *Journal of Physical Oceanography*, 40(9), 2025–2042. <https://doi.org/10.1175/2010jpo4315.1>
- Özgökmen, T. M., & Chassignet, E. P. (2002). Dynamics of two-dimensional turbulent bottom gravity currents. *Journal of Physical Oceanography*, 32(5), 1460–1478. [https://doi.org/10.1175/1520-0485\(2002\)032<1460:dotdtb>2.0.co;2](https://doi.org/10.1175/1520-0485(2002)032<1460:dotdtb>2.0.co;2)
- Padman, L., Howard, S., & Muench, R. (2006). Internal tide generation along the south scotia ridge. *Deep Sea Research Part II: Topical Studies in Oceanography*, 53(1–2), 157–171. <https://doi.org/10.1016/j.dsr2.2005.07.011>
- Park, J.-H., & Watts, D. R. (2006). Internal tides in the Southwestern Japan/East sea. *Journal of Physical Oceanography*, 36(1), 22–34. <https://doi.org/10.1175/jpo2846.1>
- Rainville, L., & Pinkel, R. (2006). Propagation of low-mode internal waves through the ocean. *Journal of Physical Oceanography*, 36(6), 1220–1236. <https://doi.org/10.1175/jpo2889.1>
- Ray, R. D. (1999). *A global ocean tide model from topex/poseidon altimetry: Got99*. 2. National Aeronautics and Space Administration, Goddard Space Flight Center.
- Renault, L., & Marchesiello, P. (2022). Ocean tides can drag the atmosphere and cause tidal winds over broad continental shelves. *Communications Earth & Environment*, 3(1), 70. <https://doi.org/10.1038/s43247-022-00403-y>
- Renault, L., Marchesiello, P., & Contreras, M. (2023). Coaction of top and bottom drags in gulf stream dynamics. *Journal of Geophysical Research: Oceans*, 128(3), e2022JC018939. <https://doi.org/10.1029/2022jc018939>
- Renault, L., Marchesiello, P., Masson, S., & McWilliams, J. C. (2019). Remarkable control of western boundary currents by eddy killing, a mechanical air-sea coupling process. *Geophysical Research Letters*, 46(5), 2743–2751. <https://doi.org/10.1029/2018gl081211>
- Renault, L., Masson, S., Arsouze, T., Madec, G., & McWilliams, J. C. (2020). Recipes for how to force oceanic model dynamics. *Journal of Advances in Modeling Earth Systems*, 12(2), e2019MS001715. <https://doi.org/10.1029/2019ms001715>
- Renault, L., McWilliams, J. C., & Gula, J. (2018). Dampening of submesoscale currents by air-sea stress coupling in the Californian upwelling system. *Scientific Reports*, 8(1), 1–8. <https://doi.org/10.1038/s41598-018-31602-3>
- Renault, L., Molemaker, M. J., Gula, J., Masson, S., & McWilliams, J. C. (2016). Control and stabilization of the gulf stream by oceanic current interaction with the atmosphere. *Journal of Physical Oceanography*, 46(11), 3439–3453. <https://doi.org/10.1175/jpo-d-16-0115.1>
- Renault, L., Molemaker, M. J., McWilliams, J. C., Shchepetkin, A. F., Lemarié, F., Chelton, D., et al. (2016). Modulation of wind work by oceanic current interaction with the atmosphere. *Journal of Physical Oceanography*, 46(6), 1685–1704. <https://doi.org/10.1175/jpo-d-15-0232.1>
- Rocha, C. B., Gille, S. T., Chereskin, T. K., & Menemenlis, D. (2016). Seasonality of submesoscale dynamics in the Kuroshio extension. *Geophysical Research Letters*, 43(21), 11–304. <https://doi.org/10.1002/2016gl071349>
- Schubert, R., Gula, J., Greatbatch, R. J., Baschek, B., & Biastoch, A. (2020). The submesoscale kinetic energy cascade: Mesoscale absorption of submesoscale mixed layer eddies and frontal downscale fluxes. *Journal of Physical Oceanography*, 50(9), 2573–2589. <https://doi.org/10.1175/jpo-d-19-0311.1>

- Scott, R. B., & Wang, F. (2005). Direct evidence of an oceanic inverse kinetic energy cascade from satellite altimetry. *Journal of Physical Oceanography*, 35(9), 1650–1666. <https://doi.org/10.1175/jpo2771.1>
- Sen, A., Scott, R. B., & Arbic, B. K. (2008). Global energy dissipation rate of deep-ocean low-frequency flows by quadratic bottom boundary layer drag: Computations from current-meter data. *Geophysical Research Letters*, 35(9), L09606. <https://doi.org/10.1029/2008gl033407>
- Shakespeare, C. J., & Taylor, J. (2014). The spontaneous generation of inertia–gravity waves during frontogenesis forced by large strain: Theory. *Journal of Fluid Mechanics*, 757, 817–853. <https://doi.org/10.1017/jfm.2014.514>
- Shchepetkin, A. F., & McWilliams, J. C. (2005). The regional oceanic modeling system (ROMS): A split-explicit, free-surface, topography-following-coordinate oceanic model. *Ocean Modelling*, 9(4), 347–404. <https://doi.org/10.1016/j.ocemod.2004.08.002>
- Simmons, H. L. (2008). Spectral modification and geographic redistribution of the semi-diurnal internal tide. *Ocean Modelling*, 21(3–4), 126–138. <https://doi.org/10.1016/j.ocemod.2008.01.002>
- Siyabolola, O. Q., Buijsman, M. C., Delpech, A., Renault, L., Barkan, R., Shriver, J. F., et al. (2023). Remote internal wave forcing of regional ocean simulations near the us west coast. *Ocean Modelling*, 181, 102154. <https://doi.org/10.1016/j.ocemod.2022.102154>
- Soufflet, Y., Marchesiello, P., Lemarié, F., Jouanno, J., Capet, X., Debret, L., & Benshila, R. (2016). On effective resolution in ocean models. *Ocean Modelling*, 98, 36–50. <https://doi.org/10.1016/j.ocemod.2015.12.004>
- Spall, M. A. (1996). Dynamics of the gulf stream/deep western boundary current crossover. Part I: Entrainment and recirculation. *Journal of Physical Oceanography*, 26(10), 2152–2168. [https://doi.org/10.1175/1520-0485\(1996\)026<2152:dotgsw>2.0.co;2](https://doi.org/10.1175/1520-0485(1996)026<2152:dotgsw>2.0.co;2)
- Srinivasan, K., Barkan, R., & McWilliams, J. C. (2022). A forward energy flux at submesoscales driven by frontogenesis. *Earth and Space Science Open Archive*, 41.
- Stewart, R. H. (2008). *Introduction to physical oceanography*. Robert H. Stewart.
- Thomas, L. N. (2012). On the effects of frontogenetic strain on symmetric instability and inertia–gravity waves. *Journal of Fluid Mechanics*, 711, 620–640. <https://doi.org/10.1017/jfm.2012.416>
- Trossman, D. S., Arbic, B. K., Straub, D. N., Richman, J. G., Chassignet, E. P., Wallcraft, A. J., & Xu, X. (2017). The role of rough topography in mediating impacts of bottom drag in eddy ocean circulation models. *Journal of Physical Oceanography*, 47(8), 1941–1959. <https://doi.org/10.1175/jpo-d-16-0229.1>
- Weatherly, G. L. (1984). An estimate of bottom frictional dissipation by gulf stream fluctuations. *Journal of Marine Research*, 42(2), 289–301. <https://doi.org/10.1357/002224084788502729>

References From the Supporting Information

- Caldwell, P., Merrifield, M., & Thompson, P. (2015). Sea level measured by tide gauges from global oceans—the joint archive for sea level holdings (NCEI accession 0019568), version 5.5, NOAA National Centers for Environmental Information, Dataset. *Centers Environ. Information, Dataset*, 10, V5V40S47W.
- Pawlowicz, R., Beardsley, B., & Lentz, S. (2002). Classical tidal harmonic analysis including error estimates in MatLab using t_tide. *Computers & Geosciences*, 28(8), 929–937. [https://doi.org/10.1016/s0098-3004\(02\)00013-4](https://doi.org/10.1016/s0098-3004(02)00013-4)